Control Engineering Practice 45 (2015) 79–85

Contents lists available at ScienceDirect

Control Engineering Practice

journal homepage: www.elsevier.com/locate/conengprac

Mars entry guidance based on segmented guidance predictor–corrector algorithm

Yuanqing Xia*, Ganghui Shen, Liuyu Zhou, Haoran Sun

School of Automation, Beijing Institute of Technology, Beijing 100081, China

ARTICLE INFO

Article history:
Received 16 February 2015
Received in revised form
15 August 2015
Accepted 15 August 2015
Available online 16 September 2015

Keywords:
Entry guidance
Predictor–corrector
Lateral control
Heading alignment

ABSTRACT

The serious challenge of future Mars mission is to find an appropriate entry guidance algorithm that can deliver the lander to the desired parachute deployment site under highly uncertain initial conditions. This paper describes the development and evaluation of the common numerical predictor–corrector algorithm and gives an improved algorithm — segmented guidance predictor–corrector algorithm for the Mars entry guidance. The common predictor–corrector algorithm can be less sensitive to initial dispersions, but needs fast on-board computation. However, the improved predictor–corrector algorithm and lateral control logic, detailed descriptions in the paper, is provided to shorten the on-board computational time. Furthermore, a heading alignment guidance law is used to improve the horizontal accuracy of the vehicle at the end of entry phase. Simulation results show that this entry guidance algorithm demonstrates reliable and robust performance in situations with high uncertainties.

1. Introduction

On August 5, 2012, the Mars Science Laboratory (MSL) entry vehicle successfully entered the Mars atmosphere and landed the rover — Curiosity safely on the surface of the planet in Gale Crater. Compared to previous unguided Mars landers, the MSL adopted active guidance algorithm during the entry phase which can decrease the errors caused by the uncertainty of atmospheric density and spacecraft aerodynamic performance, etc.

The main challenge of Martian entry is Mars' comparatively thin atmosphere (Robert & Robert, 2007). The Martian atmosphere is approximately 100 times thinner than that on the Earth, which is insufficient to provide adequate deceleration at high altitudes. Under these conditions, the vehicle's control authority will be very low. In order to ensure satisfactory delivery accuracy, some effective entry guidance algorithms were used to control the vehicle to the desired parachute deployment point in three-dimensional position space (longitude, latitude and altitude) (Prakash, Burkhart, Chen, Comeaux, & Guernsey, 2008).

There are two main entry guidance algorithms: guidance using a reference trajectory and guidance using predictor–corrector algorithm. Guidance algorithm based on a reference trajectory which is tracked during entry phase has some degrees of model-independence and does not require fast on-board computation, but it is sensitive to initial conditions. The predictor–corrector algorithm can be less sensitive to initial dispersions, but needs fast on-board computation.

The research about entry guidance algorithm using a reference trajectory started at the 1980s, Harpold and Graves (1979) firstly carried out a shuttle entry guidance based on the drag-to-velocity profile; Carman, Ives, and Geller (1998) and Mendeck and Carman (2002) presented a reference-path entry guidance method using the guidance technique of Apollo re-entry phase adapted for Mars landing conditions. In addition, Xia, Chen, Pu, and Dai (2013) and Xia and Fu (2013) developed methodology combined the active disturbance rejection control (ADRC) and slide mode control (SMC) methods, which can be used as the feedback control laws in Mars entry guidance and have shown better performances than the traditional proportional-integral-derivative (PID) law.

Kluever (2008) carried out the comparative performance analysis of pre-planned reference-path and predictive path-planning entry guidance methods for a vehicle modeled on the Mars Science Laboratory (MSL) mission, whose results showed that the reference-path tracking scheme can be easily affected by the initial condition. However, the predictive path-planning guidance can overcome the drawback.

As a result, Powell (1998) evaluated the performance of the numerical predictor–corrector technique to guide a Mars lander to both the aerocapture objective and precision landing one, namely, to deploy a parachute within 10 km of a target. Brunner and Lu (2008) and Lu (2008) carried out the skip entry guidance for lunar-return mission and used numerical predictor–corrector techniques to guide the spacecraft to the proper objectives. The main

* Corresponding author.
E-mail addresses: xia_yuanqing@bit.edu.cn (Y. Xia), hxyzsgh@gmail.com (G. Shen), sunhr1993@gmail.com (H. Sun).

http://dx.doi.org/10.1016/j.conengprac.2015.08.006
0967-0661/

Nomenclature

θ	longitude
ϕ	latitude
r	radial distance from the center of Mars
ψ	heading angle
V	velocity
γ	flight path angle
S	the vehicle's reference surface area
L	lift acceleration acting on the vehicle
D	drag acceleration acting on the vehicle
C_L	lift coefficient
C_D	drag coefficient
ρ	atmospheric density profile
g	Mars gravitational acceleration
m	the mass of vehicle
S_s	the predicted crossrange from the current position to the deployment point
S_{togo}	the angular distance between current position (θ_C, ϕ_C) and target position (θ_S, ϕ_S)
σ	bank angle
χ_c	the prespecified threshold of azimuth angle error
MSL	Mars Science Laboratory
ADRC	active disturbance rejection control
SMC	slide mode control

advantage of common predictor–corrector guidance is that it can always ensure a feasible trajectory that satisfies the required conditions from the current position to the target deployment site and find suitable bank angle magnitude which is the control variable during the entry phase to fly (Sengupta, Stelzner, Witkowski, & Rowan, 2007). However, this advantage is undermined by the increased computational time of integration and iteration. The total number of lines of code is much greater than that of other guidance algorithms.

In this paper, the authors formulate an improved algorithm — segmented guidance predictor–corrector algorithm, which is provided in this paper to shorten the on-board computational time. The improved algorithm can overcome the deficiency of common predictor–corrector guidance and could be widely used in precision guidance during the entry phase in the future.

Another contribution of the paper is that a new control law — heading alignment guidance law is adopted at the end of entry phase. In Brunner and Lu (2008) and Lu (2008), the lateral control logic is used to confine the crossrange deviation (the deviation between desired heading angle and the actual heading angle) to an acceptable velocity-dependent threshold via bank angle reversals. But the effectiveness of bank angle modulation in controlling downrange deviation becomes significantly diminished when approaching the target deployment site. In order to improve the control accuracy, we adopt the heading alignment guidance law at the end of entry phase.

This paper is organized as follows: the entry dynamic problem is formulated in Section 2. An improved predictor–corrector algorithm — segmented guidance predictor–corrector algorithm is presented in Section 3. Lateral control logic is analyzed in Section 4. Section 5 presents the heading alignment algorithm. Section 6 gives simulation results and some discussions. Finally, some concluding remarks are given in Section 7.

2. Problem formulation

Since entry duration is short and the vehicle is unpowered during the entry phase, the vehicle is modeled as a point mass flying in a planet-fixed coordinate frame. Without taking into account of the Mars' rotation, the standard simplified equations of motion for entry are (Manrique, 2010)

$$\dot{\theta} = \frac{V}{r}\frac{\cos\gamma\cos\psi}{\cos\phi} \tag{1}$$

$$\dot{\phi} = \frac{V}{r}\cos\gamma\sin\psi \tag{2}$$

$$\dot{r} = V\sin\gamma \tag{3}$$

$$\dot{V} = -D - g\sin\gamma \tag{4}$$

$$\dot{\gamma} = \frac{1}{V}\left[L\cos\sigma - \left(g - \frac{V^2}{r}\right)\cos\gamma\right] \tag{5}$$

$$\dot{\psi} = -\frac{1}{V\cos\gamma}\left[L\sin\sigma + \frac{V^2}{r}\cos^2\gamma\cos\psi\tan\phi\right] \tag{6}$$

where θ is the longitude, ϕ is the latitude, r is the radial distance from the center of Mars, V is the velocity and γ is the flight path angle, ψ is the heading angle which is the angle between the projection of the velocity on the horizontal plane and the East direction, following the counter-clockwise (ccw) from East convention (hence Eastward direction is $\psi=0°$, Northward direction is $\psi=+90°$ and Southward direction is $\psi=-90°$) (Manrique, 2010). The angles γ and ψ completely define the orientation of the velocity vector. σ is the bank angle defined as the angle from the vertical direction to the lift vector, such that a bank to the right is positive and a zero bank corresponds to the lift vector directed upward in the longitudinal plane.

The Mars gravitational acceleration is modeled as $g=\mu/r^2$, where μ is the planet's gravitational constant. In Mars, μ is approximated to 4.284e + 013. The aerodynamic forces acting on the vehicle can be decomposed into lift and drag (Robert & Robert, 2007; Mease et al., 2007). Both lift and drag are related to the vehicle's velocity, atmospheric density as well as aerodynamic coefficients. So, the drag and lift accelerations can be obtained by

$$D = \frac{1}{2}\rho V^2\frac{S}{m}C_D \tag{7}$$

$$L = \frac{1}{2}\rho V^2\frac{S}{m}C_L \tag{8}$$

where ρ is the atmospheric density, S stands for the vehicle's reference surface area and m is the mass of the vehicle. C_D and C_L represent the drag and lift coefficients, respectively. MSL adopts a scaled variation of the Viking 70° sphere-cone aeroshell and utilizes an offset center of mass to create a proper angle of attack. The aerodynamic coefficients are the typical function of the Mach number and the angle of attack. In this paper, an exponential function of the atmospheric density profile is obtained as follows:

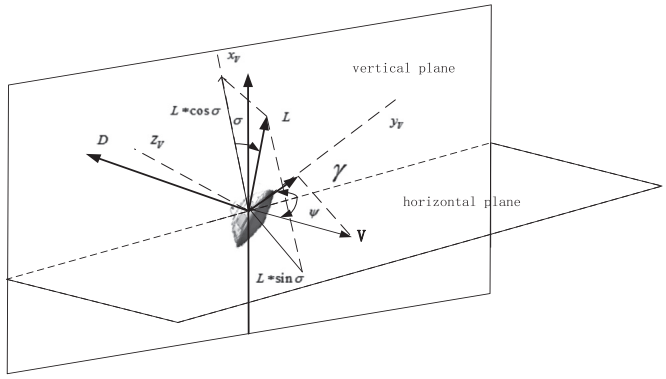

Fig. 1. Entry capsule and aerodynamic forces.

$$\rho = \rho_0 \exp^{-(r-r_0)/h_s} \tag{9}$$

where ρ_0 is the density at the reference radius r_0 and h_s is the constant scale height.

The entry bank angle and aerodynamic forces are shown in Fig. 1.

3. An improved predictor–corrector guidance algorithm

The predictor–corrector algorithm consists of a downrange (longitudinal motion) predictor–corrector one and a lateral control logic. And the downrange predictor–corrector algorithm is composed of the predictor part and corrector part. The predictor's function is to calculate the errors between the current range-to-go and the predicted range which is also called miss distance in every guidance cycle via the predictor, then find and output a command bank angle magnitude which satisfies the requirement that the current range-to-go and the predicted range are equal via corrector. In addition, the predicted crossrange miss is compared to the estimated lateral control capability, and a reversal is performed when the predicted miss is equal to half of the lateral control capability. In this paper, another lateral control logic will be discussed later.

3.1. The common longitudinal predictor–corrector guidance approach

3.1.1. Predictor process

The main purpose in the predictor process is to calculate the range-to-go S_{togo} and the predicted range S_s. The range-to-go S_{togo} is decided by the longitude and latitude of the current place and the target deployment place. The range-to-go can be obtained by (Brunner & Lu, 2008; Lu, 2006)

$$S_{togo} = \arccos(\sin\theta_C \sin\theta_S + \cos\theta_C \cos\theta_S \cos(\phi_C - \phi_S)) \tag{10}$$

where C and S are the current and target positions, respectively. θ_C, θ_S, ϕ_C, ϕ_S are the longitude and latitude of positions C and S, respectively.

Furthermore, if the bank angle σ is determined, we can obtain the predicted range S_s from the current position to the deployment point by integrating the equation:

$$\dot{s} = \frac{V\cos\gamma}{r} \tag{11}$$

and the entry dynamic equations (Eqs. (1)–(6)). Then we can get the error between the range-to-go S_{togo} and the predicted range S_s. Note that the bank angle is needed in every guidance cycle of prediction in order to integrate the dynamic equations and get the predicted range, so a future bank angle planning is needed in predictor process, which can be called bank angle strategy. The bank angle strategy proposed by Brunner and Lu (2008) is a more robust strategy.

3.1.2. Corrector process

The purpose of the corrector process is that when the downrange deviation does not meet the requirement, the bank angle should be corrected to make the downrange deviation small enough. A secant iteration scheme is employed to find the required bank-angle magnitude. The iterates are generated by the equation (Brunner & Lu, 2008)

$$\cos\sigma_{n+1} = \cos\sigma_n - \frac{\cos\sigma_n - \cos\sigma_{n-1}}{\triangle_S(\sigma_n) - \triangle_S(\sigma_{n-1})}\triangle_S(\sigma_n) \tag{12}$$

where $\triangle_S(\sigma_n) = S_{togo} - S_s$. It is clear from the above equation that two predicted downrange deviations are needed to get the new bank angle magnitude in this process.

To start the secant iteration scheme appropriately for the first time, an initial guess of the bank angle is required. Considering that large bank angle can meet the constraints on heat load, heat rate and deceleration load, we assume that an initial bank angle of 60° is used in the numerical simulation of the trajectory. After the first guidance cycle, the previously calculated bank angle is used as an initial angle rather than beginning with a 60° bank angle. If this angle is still sufficient to bring the downrange deviation within accepted tolerance, the secant method is skipped and the previous bank angle is flown. Otherwise, the secant method proceeds as already noted and determines a new bank-angle magnitude.

3.2. An improved algorithm — segmented guidance predictor–corrector algorithm

Although the predictor–corrector algorithm discussed above has a great performance in precision guidance (see simulation results below), it has not been used in real guidance practice until now. A main reason is that current computational devices onboard may not satisfy the requirement of the large computational time needed for this algorithm. With the development of technology, the high-speed devices which satisfy the requirement may come into use someday. Another way to solve this problem is that we improve this predictor–corrector algorithm to reduce the computational time. Incorporating the advantage of the trajectory tracking and predictor–corrector guidance, segmented guidance based on predictor–corrector algorithm is presented in this paper as an effective way to reduce the computational time. The segmented guidance is as follows:

(1) According to the predicted entry position and the target deployment site, a reference trajectory is planned prior to the entry phase.
(2) Several points in this reference trajectory are selected as the segmented target points to be tracked.
(3) The predictor–corrector algorithm, which has been described in detail in the previous section, is used between every two consecutive points been selected in the previous step. So the vehicle will always head for the next point via predictor–corrector algorithm.

The reference trajectory can be pre-planned by many optimizing methods, such as the Gauss pseudo-spectral method. And the number of selected points should be considered carefully. If too many points are selected, the time will not be enough for every segment to execute predictor–corrector algorithm, so the guidance accuracy will be seriously undermined. On the contrary, if only one or two points are selected, the total computational time may not be significantly reduced.

Range can be chosen as the trigger of changing phase. When the range from the last changing phase point to the current position is equal to the range-to-go between two pre-selected points closely, the vehicle will switch to the next phase, heading for the next point.

This segmented guidance not only preserves the advantage of the classic predictor–corrector algorithm in that it is not so much sensitive to initial dispersions, but it also significantly reduces the total computational time of integration.

4. Lateral control logic

The longitudinal predictor–corrector algorithm can only obtain the magnitude of bank angle. Thus, we use a lateral control logic to get the sign of bank angle. By using the lateral control logic, the crossrange deviation can be confined into an acceptable bound via bank angle reversals (Shen & Lu, 2004). There are mainly two methods of lateral control for low lift-to-drag (L/D) ratio vehicles:

(1) Bank reversal based on crossrange error.
(2) Bank reversal based on azimuth angle error.

These two methods are similar in that when the error (crossrange error or azimuth angle error) exceeds the prespecified threshold, the sign of bank angle is reversed. In the paper, We mainly introduce the latter. An azimuth angle threshold is defined as a quadratic or simply a linear function of the dimensionless velocity (Xue & Lu, 2009):

$$\chi_c = c_1 V + c_0 \tag{13}$$

$$\chi = \arcsin(\sin S_{togo} \sin(\psi - \Psi)) \tag{14}$$

where S_{togo} is the range-to-go, ψ is the current heading angle, and Ψ is the line-of-sight azimuth angle along a great circle to the parachute deployment site. All the variables have units of radians. Note that the definition of heading angle discussed in this paper is different from other previous works, the computation method of heading angle error is given as follows (Manrique, 2010):

In Fig. 2, the point N corresponds to the North Pole of the planet, characterized by an indeterminate longitude and latitude of 90°. The distance d_{12} can be found by

$$d_{12} = \arccos(\cos\phi_1 \cos\phi_2 \cos(\theta_1 - \theta_2) + \sin\phi_1 \sin\phi_2) \tag{15}$$

The angle φ can be obtained by

$$\varphi = \arccos\frac{\sin\phi_2 - \sin\phi_1 \cos d_{12}}{\cos\phi_1 \sin d_{12}} \tag{16}$$

The desired heading angle of the great circle between p_1 and p_2 is

$$\psi_d = \pi/2 - \varphi \tag{17}$$

Detailed description of calculating the desired heading angle can be found in Manrique (2010). So the heading angle error is

$$\triangle_\psi = \psi - \psi_d \tag{18}$$

If the heading angle error exceeds the prespecified threshold, the lateral control logic reverses the sign of bank angle, otherwise the sign of bank angle will keep. The core of this method is to make the vehicle directly fly to the target deployment site.

In the trajectory planning, the change of the bank-angle sign is achieved instantaneously. However, this cannot be done in real situation because of the limit of rate and acceleration. The time required to perform the bank reversals is a function of the current bank angle magnitude and the roll axis, which is the response of the flight control system (Carman et al., 1998). As in the Apollo guidance, the loss of closed loop drag and altitude rate control are disadvantages of using discrete bank reversals to control crossrange. So for optimum range control, the number of reversals must be minimized, consistent with preserving acceptable crossrange control.

Fig. 3 shows the relationship between crossrange error and its threshold using the common algorithm (including the lateral control logic). The change of bank angle is presented in Fig. 4. They show that when approaching the target site, the sign of bank angle is reversed frequently and the bank angle is also large in that period. But the effectiveness of bank angle modulation in controlling crossrange deviation becomes significantly diminished when approaching the target deployment site (Jody, Cianciolo, Powell, & Shidner, 2010). So in the final entry phase, a heading alignment controller is initiated which aligns the vehicle velocity heading with the target instead of lateral control logic, nulling the crossrange error when the target is reached.

5. Heading alignment

A heading alignment guidance law following the feedback linearization procedure is presented in this section. The goal of this guidance is to drive the heading angle error to zero. The heading angle error is defined in the previous section:

$$e(t) = \psi(t) - \psi_d(t) \tag{19}$$

where $\psi(t)$ is the current heading angle and $\psi_d(t)$ is the desired

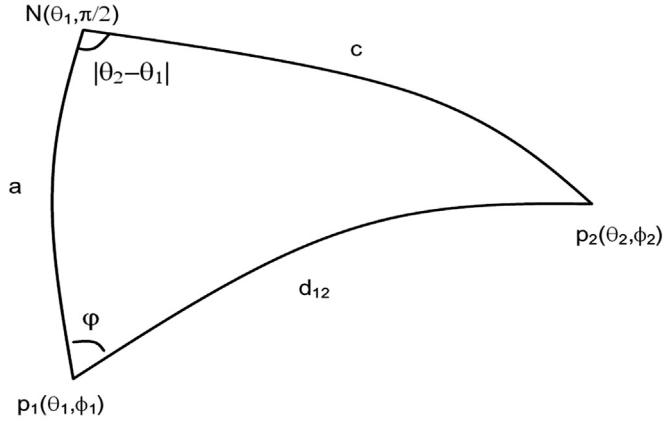

Fig. 2. Spherical triangle.

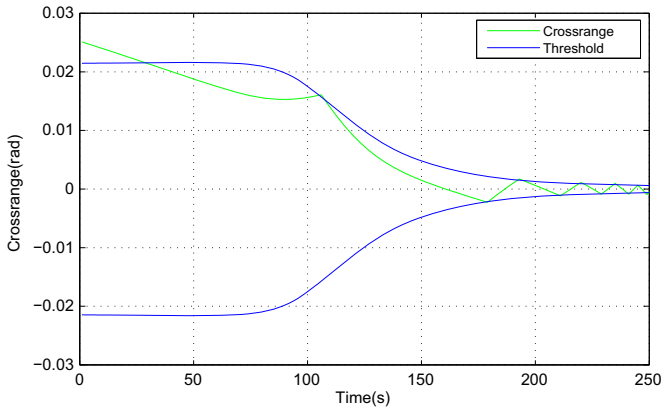

Fig. 3. Crossrange and threshold using the common algorithm.

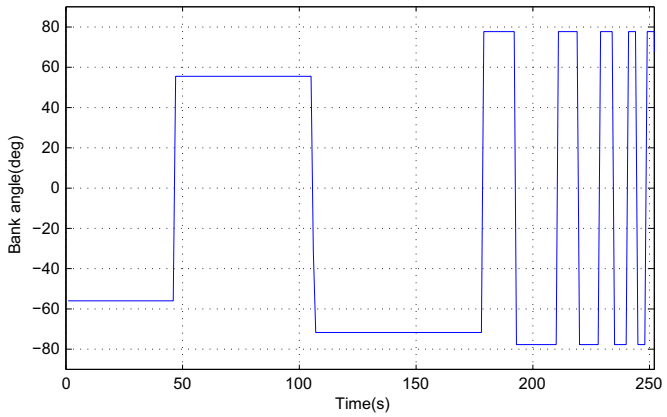

Fig. 4. The bank angle using the common algorithm.

heading angle. The desired heading angle $\psi_d(t)$ is obtained from Eqs. (15) to (17).

Following the standard feedback linearization procedure, we specify the desired first order error dynamics (Manrique, 2010)

$$\dot{e}(t) + k_1 e(t) = 0 \tag{20}$$

With $k_1 > 0$, the error goes to zero asymptotically. After substituting the heading dynamics in Eq. (6), the required guidance law is found to be

$$\sin\sigma = -\frac{V\cos\gamma}{L}[-k_1(\psi(t) - \psi_d(t)) + \dot{\psi}_d(t)] \tag{21}$$

Without saturation and modeling errors, this guidance law will lead to the error behavior

$$e(t) = e(0)e^{-k_1 t} \tag{22}$$

k_1 should be 3–5 times the inverse of the remaining time-to-go. If we want to change k_1 to adjust the final altitude, we may have to trade off horizontal accuracy for vertical accuracy (Manrique, 2010). In order to increase the deployment altitude while still allowing some reduction of crossrange errors, the commanded bank angle is not allowed to go beyond 85° magnitude in this phase. Simulation results show that this method is effective in controlling heading angle.

Therefore, the proposed algorithm (the improved guidance strategy) is shown in Fig. 5 using a block diagram. At first the segmented guidance is used between every two consecutive target points to obtain the magnitude of bank angle and a lateral control logic is adopted to determine the sign of bank angle at the same time. In order to improve the landing accuracy, the heading alignment guidance law mentioned above is applied to control the vehicle flying to the desired parachute deployment point in the final entry phase.

6. Simulation results

In this paper, we choose the information of the MSL as the numerical calculation, and the parameters taken to perform the simulation come mostly from the MSL lander's data (such as Tables 1–4). The nominal initial conditions of the vehicle are shown in Table 1, and the target conditions are shown in Table 2. The reference surface area of the vehicle is 15.9 m^2, and the mass profile of the spacecraft is 2804 kg.

Due to the requirement of high landing altitude, the parachute is deployed when the altitude ranges from 7 to 12 km. Past missions to Mars have triggered parachute deployment at a specific velocity. In this paper, the simulation is terminated when the velocity of the vehicle is less than 400 m/s or the altitude is below 7 km.

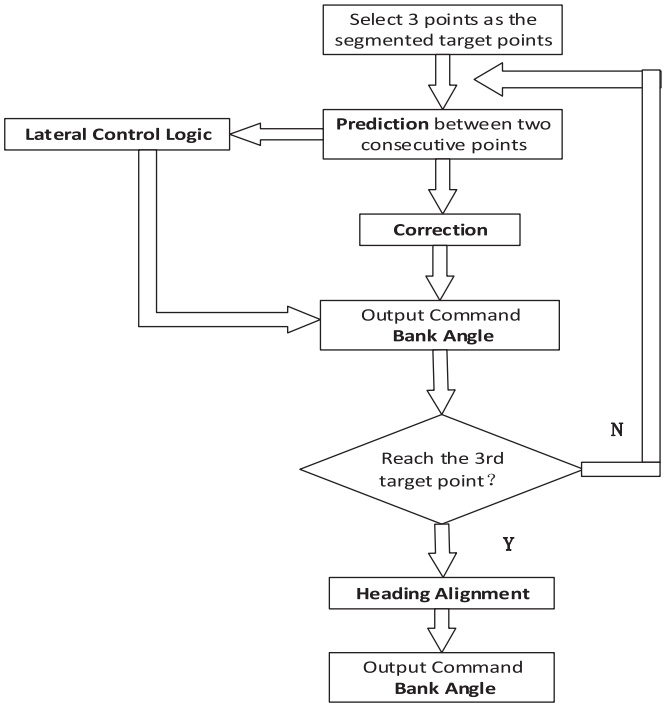

Fig. 5. The block diagram of the proposed algorithm.

Table 1
Initial conditions.

State variable	Value
θ_0	−90.07°
ϕ_0	−43.8°
r_0	3520.76 km
ψ_0	4.99°
V_0	5505 m/s
γ_0	−14.15°

Table 2
Target conditions.

State variable	Value
θ_f	−73.26°
ϕ_f	−41.45°
h_f	7 km

Table 3
Terminal conditions.

State variable	Predictor–corrector	Segmented guidance
θ_f	−73.259°	−73.214°
ϕ_f	−41.450°	−41.434°
h_f	8.30 km	7.00 km
V_f	458.08 m/s	425.69 m/s
Simulation time	3.205 s	1.914 s

Fig. 6 shows the relationship between crossrange errors and its threshold using the segmented guidance and a heading alignment guidance. And the change of bank angle is presented in Fig. 7. Compared to Fig. 4, Fig. 7 indicates that the reverse of bank angle is less.

Fig. 8 shows total trajectories when executing common predictor–corrector algorithm and the improved guidance strategy

Table 4
Initial state dispersions.

State variable	Mean	3σ
θ_0	$-90.07°$	0.3°
ϕ_0	$-43.8°$	0.03°
r_0	3520.76 km	2.306 km
ψ_0	4.99°	0.23°
V_0	5505 m/s	2.85 m/s
γ_0	$-14.15°$	0.15°

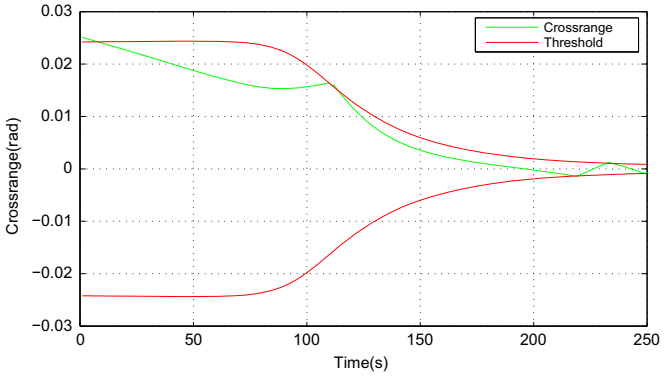

Fig. 6. Crossrange and threshold using the segmented guidance and a heading alignment guidance law.

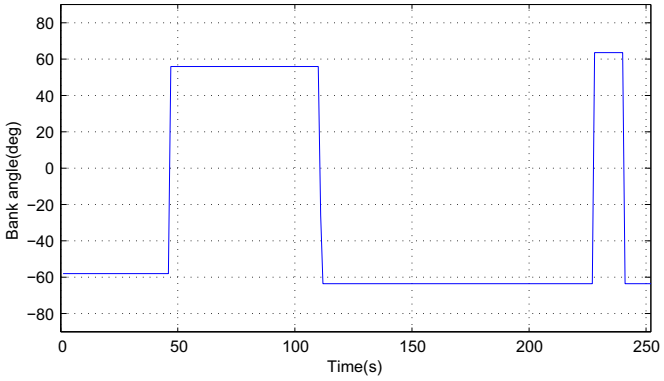

Fig. 7. The bank angle using the segmented guidance and a heading alignment guidance law.

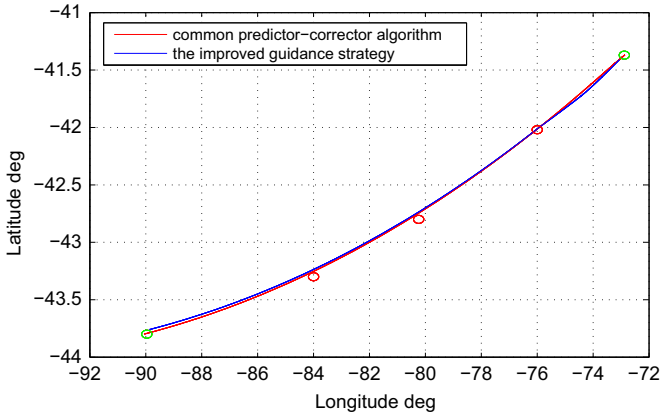

Fig. 8. Trajectories of common predictor–corrector algorithm and the improved guidance strategy.

(including segmented guidance predictor–corrector algorithm and heading alignment guidance). Trajectory using the improved guidance strategy is blue in the figure.

As for the blue line, there are 3 points selected on a pre-planned trajectory. The coordinates of the 3 points are ($-84°$, $-43.26°$), ($-80.24°$, $-42.75°$) and ($-76°$, $-42.02°$). In the first 3 phases, the vehicle flies with segmented guidance, then the vehicle switches to the heading alignment guidance in the last phase, heading for the target.

Fig. 8 has shown that the overall performance of the predictor–corrector algorithm is perfect in that it can drive the vehicle to the exact target deployment site with only little error. It is also shown that the segmented guidance can head for the 3 selected points successively. Simulation results show that the segmented guidance can also meet the precision landing requirement.

In addition, the simulation is conducted on a computer with an Intel Core 2 Duo T6600, 2.2 GHz CPU. And the guidance cycle is set to 1 s. Simulation time of the segmented guidance is about half of the time with predictor–corrector algorithm (shown in Table 3), which proves that the segmented guidance can reduce the computational time. With more points selected, the computational time will be significantly reduced. The achieved deploying conditions of the predictor–corrector algorithm and segmented guidance are shown in Table 3.

In order to assess the robustness and reliability of the predictor–corrector algorithm and its improved one — segmented guidance, Monte Carlos with 100-dispersed cases were run using MATLAB simulation for the two guidance algorithms. These dispersions and modeling errors are representative of current capability and knowledge. The means and the standard deviations for the initial state variables are shown in Table 4. In this paper, considering the high uncertainties and the limited knowledge of human about Martian atmosphere, atmospheric model errors and wind influence are considered to be the atmospheric density errors. This is reasonable because the atmospheric model errors and wind influence can change the vehicle's position mainly by changing the lift and drag forces, which are the functions of the atmospheric density. And the errors in the lift and drag coefficients which are the functions of Mach number are also included in atmospheric density errors. The standard deviation for the atmospheric density is set equal to 30 percent of the normal conditions.

The Monte Carlo results for the predictor–corrector algorithm are shown in Fig. 9, the segmented guidance and heading alignment guidance law are shown in Fig. 10. The circles are distances of 5 km and 10 km from target.

The results in Fig. 9 show that almost 73 percent of the cases based on predictor–corrector algorithm have ranges from target within 5 km, while 98 percent are within 10 km. The deployment accuracy is better based on segmented guidance and heading alignment with 86 percent of the cases within 5 km and 100

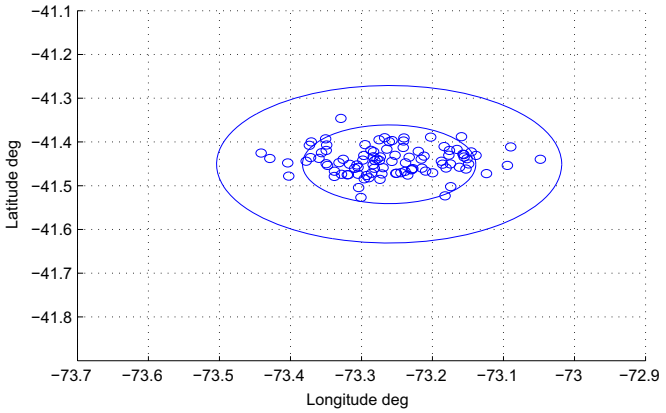

Fig. 9. Deployment positions using predictor–corrector algorithm.

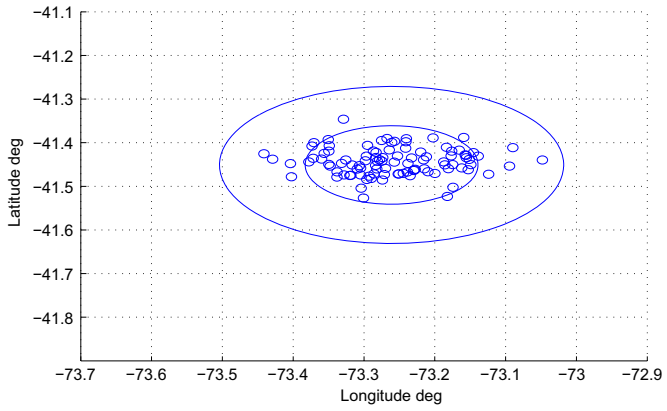

Fig. 10. Deployment positions using segmented guidance and heading alignment.

percent within 10 km.

The mean crossrange deviation of the two guidance algorithms are nearly the same which proves that the segmented guidance and heading alignment can effectively control the crossrange deviation within a specific tolerance as the predictor–corrector algorithm. Note that all the deployment positions in this simulation have an altitude above 7 km which can help to satisfy the high-elevation landing requirement. And it is decided by the deployment trigger logic designed in the beginning of this section. So if the deployment trigger logic is improved to enhance the horizontal accuracy, the crossrange deviation will be further mitigated.

As a result, simulation shows that the predictor–corrector algorithm and the improved guidance strategy (the segmented guidance and heading alignment) have robust and reliable performances in situations with high uncertainties and can achieve precision landing requirement. And the less simulation time of the segmented guidance indicates that it can significantly reduce the on-board computational time in real practice.

7. Conclusions

In this paper, a predictor–corrector guidance algorithm for the very low lift-to-drag ratio Mars lander, modified on the basis of the skip entry guidance for lunar-return mission carried out by Brunner and Lu has been presented. This guidance strategy includes a longitudinal predictor–corrector algorithm and lateral control logic. The magnitude of bank angle can be automatically changed to meet the downrange deviation requirement. The sign of bank angle is reversed when the heading angle error exceeds the pre-selected threshold. In order to control the deployment of the vehicle, a heading alignment controller drives the vehicle heading for the target instead of predictor–corrector algorithm at the end of the entry phase.

Moreover, an improved predictor–corrector algorithm called segmented guidance is proposed to reduce the large on-board computational time of integration. Simulation results show that the performances of both the predictor–corrector algorithm and segmented guidance are good in ensuring precision landing requirement and the segmented guidance algorithm can significantly reduce the computational time.

Acknowledgment

The authors would like to thank the referees for their valuable and helpful comments which have improved the presentation. The work was supported by the National Basic Research Program of China (973 Program) (2012CB720000), the National Natural Science Foundation of China (61225015), Foundation for Innovative Research Groups of the National Natural Science Foundation of China (Grant no. 61321002).

References

Brunner, C. W., & Lu, P. (2008). Skip entry trajectory planning and guidance. *Journal of Guidance Control and Dynamics*, *31*(5), 1210–1219.

Carman, G. L., Ives, D. G., & Geller, D. K. (1998). Apollo-derived Mars precision landing guidance. In *Proceedings of the AIAA atmospheric flight mechanics conference* 98-4570, Boston, MA, August 10–12.

Harpold, J. C., & Graves, C. A. (1979). Shuttle entry guidance. *Journal of the Astronautical Sciences*, *37*(3), 239–268.

Jody, L. D., Cianciolo, A. D., Powell, R. W., & Shidner, J. D. (2010). Guidance and control algorithms for the Mars entry, descent and landing systems analysis. In *Proceedings of the astrodynamics specialist conference* 2010-7972, Toronto, Ontario Canada, August 2–5.

Kluever, C. A. (2008). Entry guidance performance for Mars precision landing. *Journal of Guidance, Control, and Dynamics*, *31*(6), 1537–1544.

Lu, P. (2006). Asymptotic analysis of quasi-equilibrium glide in lifting entry flight. *Journal of Guidance, Control, and Dynamics*, *29*(3), 662–670.

Lu, P. (2008). Predictor–corrector entry guidance for low-lifting vehicles. *Journal of Guidance, Control, and Dynamics*, *31*(4), 1067–1075.

Manrique, J. B. (2010). Advances in spacecraft atmospheric entry guidance (Ph.D. thesis). Irvine, California, USA: University of California, Irvine.

Mease, K. D., Leavitt, J. A., Benito, J., & Talole, S. (2007). Advanced hypersonic entry guidance for Mars pinpoint landing. In *Proceedings of the NASA science technology conference*. MD, USA: University of Maryland University College, June 19–21.

Mendeck, G. F., & Carman, G. L. (2002). Guidance design for Mars Smart Landers using the entry terminal point controller. In *Proceedings of the AIAA atmospheric flight mechanics conference* 2002-4502, Monterey, California, August 5–8.

Powell, R. W. (1998). Numerical roll reversal predictor–corrector aerocapture and precision landing guidance algorithm for Mars surveyor program 2001 missions. In *AIAA atmospheric flight mechanics conference* 1998-4574, Boston, MA, August 5–8.

Prakash, R., Burkhart, P. D., Chen, A., Comeaux, K. A., & Guernsey, C. S. (2008). Mars science laboratory entry, descent, and landing system overview. In *IEEE aerospace conference* 2008-1531.

Robert, D. B., & Robert, M. M. (2007). Mars exploration entry, descent, and landing challenges. *Journal of Spacecraft and Rockets*, *44*(2), 310–323.

Sengupta, A., Stelzner, A., Witkowski, A., & Rowan, J. (2007). An overview of the Mars science laboratory parachute decelerator system. In *Proceedings of the AIAA aerospace conference* 2007-2578, Williamsburg, VA, May 21–24.

Shen, Z., & Lu, P. (2004). Dynamic lateral entry guidance logic. *Journal of Guidance, Control, and Dynamics*, *27*(6), 949–959.

Xia, Y. Q., Chen, R. F., Pu, F., & Dai, L. (2013). Active disturbance rejection control for drag tracking in Mars entry guidance. *Advances in Space Research*, *53*(5), 853–861.

Xia, Y. Q., & Fu, M. Y. (2013). *Compound control methodology for flight vehicles*. Berlin, New York: Springer.

Xue, S. B., & Lu, P. (2009). Constrained predictor–corrector entry guidance. In *AIAA guidance navigation and control conference* (Vol. 33(4), pp. 1273–1281).